JOURNAL OF MATERIALS SCIENCE 23 (1988) 2174–2180

Dislocation structures in deformed Cu–Ni–Zn alloy single crystals

TAICHIRO ITO, YUTAKA NAKAYAMA
College of Engineering, University of Osaka Prefecture, Mozu-Umemachi, Sakai, Osaka 591, Japan

It is known that Cu–Ni–Zn alloy has an ordered structure Cu_2NiZn (Ll_2) by annealing between 573 and 623 K. In the present experiments, the effects of annealing on the dislocation structure were studied on Cu–Ni–Zn single crystals with several compositions. Thin foils cut parallel to the {1 1 1} planes were observed in a transmission electron microscope. The results obtained are as follows. (i) In Cu–5Ni–5Zn, Cu–10Ni–10Zn and Cu–15Ni–15Zn (at%), the stress–strain behaviour, slip mode and dislocation structure did not change by annealing at 573 K. However, the slip mode became more concentrated and localized, and dislocations emitted from a source tended to stay on the same slip plane, as the nickel and zinc concentrations increased. (ii) However, those properties in Cu–20Ni–20Zn and Cu–25Ni–25Zn changed drastically by annealing. As the ordering proceeded, uniform distributions of superlattice dislocations were observed. A typical dislocation configuration, with long screw and wavy-edged superlattice dislocations, took the place of piled-up unit dislocations. (iii) The facts that edge-type superlattice dislocations formed dipoles and their clusters, and that the secondary dislocation density was much lower than the primary one, implied that the elastic interaction of the primary edge-type superlattice dislocations on the nearby parallel slip planes would control the work-hardening of ordered Cu_2NiZn alloy single crystals.

1. Introduction

Since the existence of Ll_2-type long-range order in Cu_2NiZn was confirmed by neutron diffraction, superlattice dislocations and antiphase domain boundaries were observed in deformed Cu_2NiZn by means of transmission electron microscopy [1–9]. The mechanical properties of polycrystalline and single-crystal Cu–Ni–Zn alloys with several compositions were also examined, in relation to annealing and deformation temperatures. In accordance with the results from neutron diffraction, the most predominant features in the mechanical properties were obtained in Cu–20Ni–20Zn and Cu–25Ni–25Zn by annealing at 573 K, though the mechanical properties did not change by annealing in Cu–15Ni–15Zn [4–6]. As only a restricted number of reports have been published on the effects of ordering on the dislocation structure for polycrystalline [9] and single-crystal Cu–Ni–Zn alloys [4–6], more detailed study on the dislocation structure of single crystals is necessary to understand the deformation characteristics of Cu–Ni–Zn alloys.

The present study aims to determine the characteristics of the deformed structure of Cu–Ni–Zn alloy single crystals with several compositions. Thin foils cut parallel to the primary slip plane and other special planes were observed in a transmission electron microscope (TEM). In particular, emphasis was placed on the effects of annealing on the dislocation structure of the more concentrated Cu–Ni–Zn alloys.

2. Experimental procedure

99.99% copper and zinc and 99.9% nickel were melted together to obtain five kinds of Cu–Ni–Zn alloys with the composition of $Cu_{1-2x}Ni_xZn_x$. The chemical composition are listed in Table I. After being homogenized at 1173 K for 600 ksec, ingots were cold-rolled to plates of 4 mm thickness. Single crystals of 4 mm × 4 mm × 200 mm were grown from the melt by the Bridgman method under an argon gas atmosphere.

Prior to determining the orientation of crystals by the Laue method, they were homogenized at 1173 K for 90 ksec under an argon gas atmosphere. From the central part of crystals with a single slip orientation, two specimens of 60 mm length were cut using an acid sawing machine. All of them were quenched from 1073 K to obtain a homogeneous solid solution. Furthermore, some of them were annealed at 573 K for up to 360 ksec in Pyrex tubes filled with argon gas. Specimens were chemically and electrolytically polished to the shape of tensile specimens with a gauge length of 40 mm and cross-section of 3.5 mm × 3.5 mm. They

TABLE I Compositions of Cu–Ni–Zn alloys

Alloy No.	Composition (at%)		
	Cu	Ni	Zn
NZ-0505	90.2	5.1	4.7 (balance)
NZ-1010	79.6	9.8	10.6 (balance)
NZ-1515	69.8	15.0	15.2 (balance)
NZ-2020	59.5	19.8	20.7 (balance)
NZ-2525	48.9	24.4	26.7 (balance)

0022–2461/88 $03.00 + .12

were stretched 10% with an initial strain rate of $2.1 \times 10^{-4}\,sec^{-1}$. Slip lines on the top surface, which is nearly perpendicular to the slip direction (deviation at most 0.26 rad) were observed on carbon replicas shadowed with germanium in the TEM. To observe the dislocation structure, discs parallel to the primary slip plane (1 1 1) and the cross-slip plane (1 $\bar{1}$ 1) were cut using the acid sawing machine. They were polished to thin foils, and observed in the TEM operated at 200 kV.

3. Results

3.1. Shear stress–shear strain curves

Shear stress–shear strain curves for Cu–Ni–Zn alloy single crystals deformed at room temperature up to 10% are shown in Fig. 1. Crystals quenched from 1073 K exhibit sharp yield drops and a very low work-hardening rate in Stage 1 corresponding to the Lüders type of deformation, except NZ-0505 which does not show the yield drop. The effects of annealing on the stress–strain behaviour seem negligible for NZ-0505 and NZ-1010. NZ-1515 when annealed has a little higher stress level than the quenched sample, but the difference between them is within the experimental fluctuation among crystals. On the other hand, in NZ-2020 and NZ-2525 the critical resolved shear stress (CRSS) and the work-hardening rate in Stage 1 are increased remarkably by annealing.

The effects of annealing on CRSS are shown in Fig. 2 for NZ-2020 and NZ-2525 single crystals. The CRSS increases rapidly until 0.36 ksec and continues to increase slowly at least until 360 ksec.

3.2. Observation of slip lines

Electron replica micrographs of surface slip lines were observed. In NZ-0505, NZ-1010 and NZ-1515, slip lines tend to be coarse and localized as the solute concentration increases. It is not easy to detect any difference in the distribution, shape and width of slip lines between the quenched and annealed (360 ksec) states. On the other hand, the slip lines on NZ-2020 and NZ-2525 change remarkably on annealing, as shown in Fig. 3. In the quenched state the slip lines are very coarse, localized and widely scattered in width. In NZ-2020 annealed for 3.6 ksec, the slip lines exhibit high contrast compared with those in the quenched state. Most of the slip lines become fine; however, the individual slip lines can still be resolved. After annealing for more than 36 ksec, the slip lines become very fine and it is hard to distinguish individual slip lines.

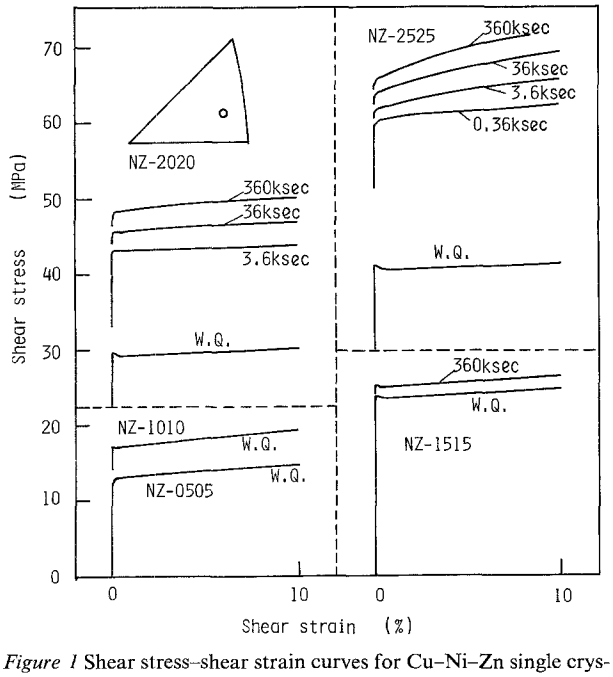

Figure 1 Shear stress–shear strain curves for Cu–Ni–Zn single crystals annealed at 573 K for various periods. W.Q. = water-quenched.

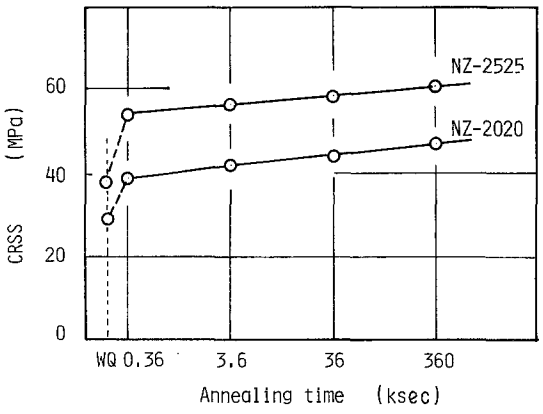

Figure 2 The relation between CRSS and annealing period at 573 K for NZ-2020 and NZ-2525. WQ = water-quenched.

In NZ-2525, the slip lines in the quenched state become more localized and concentrated than in NZ-2020. However, by annealing only for 0.36 ksec the slip lines become fine, diffused and distributed uniformly. More than 98% of the total slip is due to fine slip lines with a height less than 10 nm, which is the limit of resolution; however, a small number of clustered slip lines still exist. By annealing for more than 3.6 ksec, the individual slip lines become too fine and diffused to be resolved. The change in the slip mode in the present alloys is similar to Cu_3Au and Ni_3Mn [10, 11].

3.3. Observation of dislocation structure

3.3.1. NZ-0505, NZ-1010 and NZ-1515

A typical dislocation structure in a section parallel to the (1 1 1) plane of NZ-0505 is shown in Fig. 4. Small dislocation loops are distributed all around the specimen, which would be formed by condensation of quenched-in vacancies during annealing at 573 K. They interact with moving dislocations; however, the overall dislocation structure does not seem to be changed by their existence. Long primary dislocations distribute uniformly with equal spacing. Most of the dislocations have edge or near-edge characters and there are elastic interaction between dislocations on nearby slip planes.

As the solute concentration increases, primary dislocations tend to stay on their own slip planes with smaller spacings, as in copper solid solutions which show a decrease in stacking fault energy with an increase in solute concentration [12].

3.3.2. NZ-2020

In the quenched state, the slip-line pattern predicts the existence of typical piled-up arrays of dislocations. Fig. 5 shows a (1 1 1) section including a slip band.

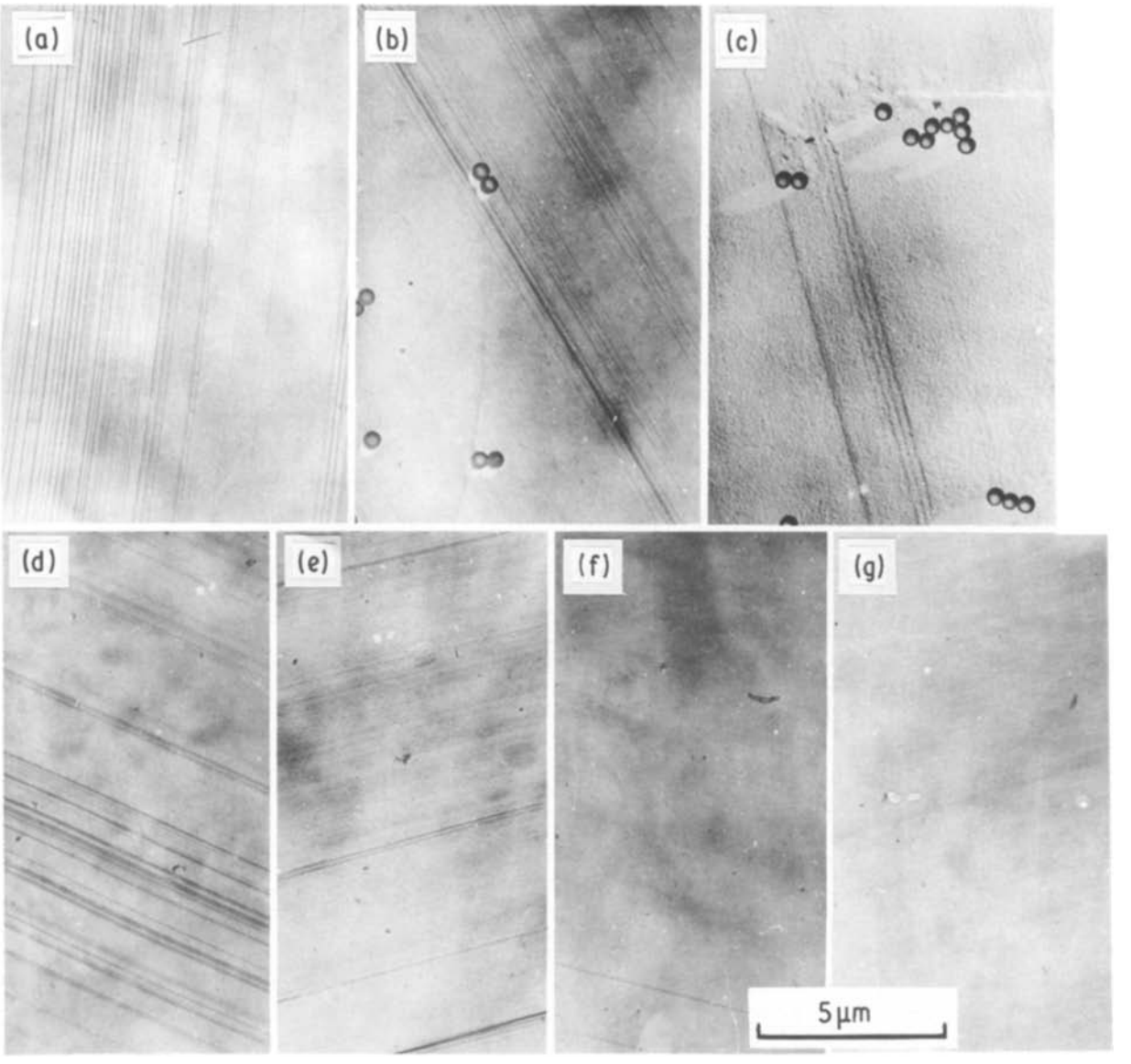

Figure 3 Electron replica micrographs of slip lines for NZ-2020 and NZ-2525 annealed at 573 K: (a) NZ-2020 water-quenched, (b) NZ-2020 3.6 ksec, (c) NZ-2020 360 ksec, (d) NZ-2525 water-quenched, (e) NZ-2525 0.36 ksec, (f) NZ-2525 3.6 ksec, (g) NZ-2525 360 ksec.

Primary dislocations generated from a source have a strong tendency to stay on the same slip plane. The separation of dislocations in a piled-up array becomes narrower and the number of dislocations generated from a source become larger than in the dilute alloys.

Fig. 6 shows the dislocation structure in a (1 1 1) section of a crystal annealed for 3.6 ksec. There are two kinds of dislocation structure: uniform piled-up arrays of unit dislocations which have elastic interaction with those on parallel slip planes, and isolated long wavy dislocations which form pairs on the same slip plane.

After annealing for 360 ksec, dislocations arrange and distribute uniformly. Most of dislocations form pairs and are wavy. The features in the dislocation structure are similar to those in the annealed NZ-2525.

3.3.3. NZ-2525

In the quenched state, the dislocation structure is similar to that in NZ-2020. By annealing only for 0.36 ksec, the dislocation structure changes to a transition structure from the piled-up to the uniform arrangement. Fig. 7 shows the typical structure. In some parts a uniform distribution of superlattice dislocations is observed, similar to that in specimens annealed for longer periods. In other parts, concentrated piled-up arrays of unit dislocations are observed. These dislocation structures correspond well to the coexistence of fine and clustered slip lines observed in Fig. 3.

By annealing for more than 3.6 ksec the dislocation structure becomes similar to that for specimens annealed for 360 ksec, which is shown in Fig. 8. There are long screw-type superlattice dislocations. Connecting them, wavy edge-type superlattice dislocations are forming dipoles and their clusters. In Fig. 9, the dislocation structure on a (1 $\bar{1}$ 1) section is observed. Dislocations are distributing rather uniformly, though regions with high dislocation density (marked A in the figure) are observed. Almost all short edge dislocations are forming pairs. The regions with edge superlattice dislocation dipole clusters in Fig. 8 will corresponding to the regions with high dislocation density in Fig. 9. The impressive point in these figures is that the density of dislocations belonging to secondary slip

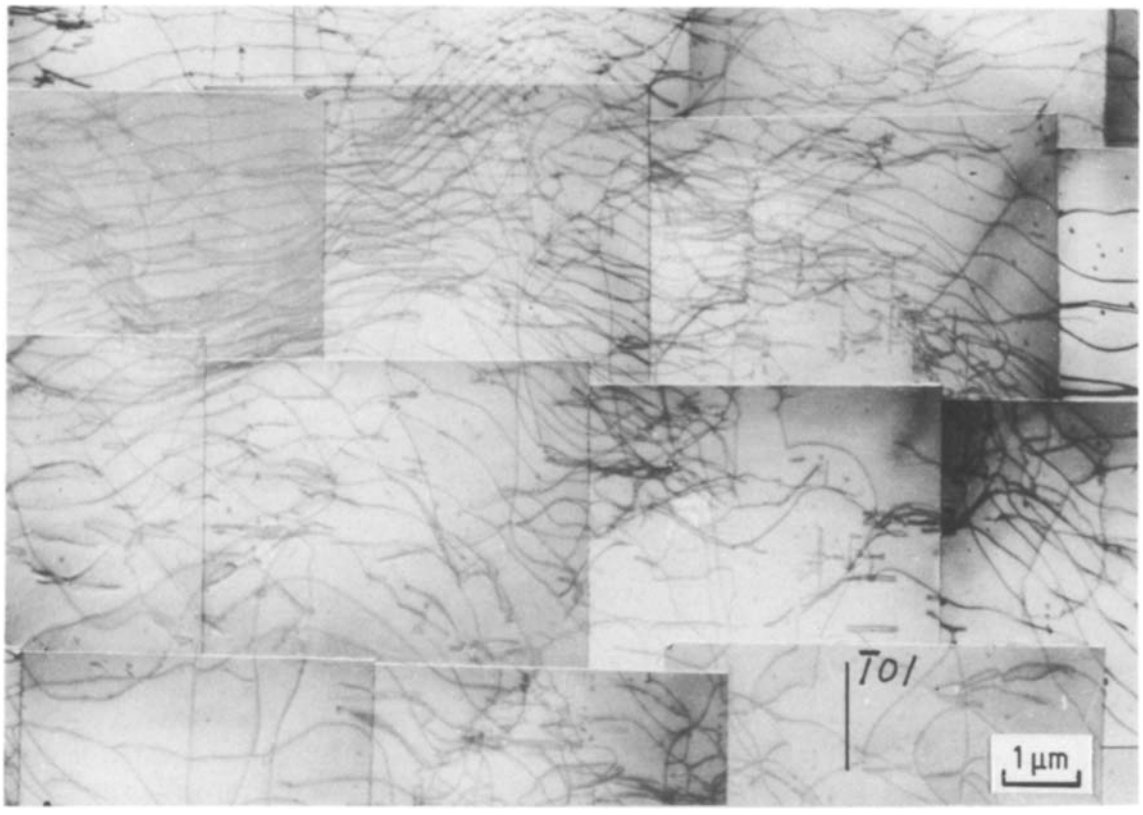

Figure 4 Transmission electron micrograph for NZ-0505 annealed at 573 K for 360 ksec. (1 1 1) foil.

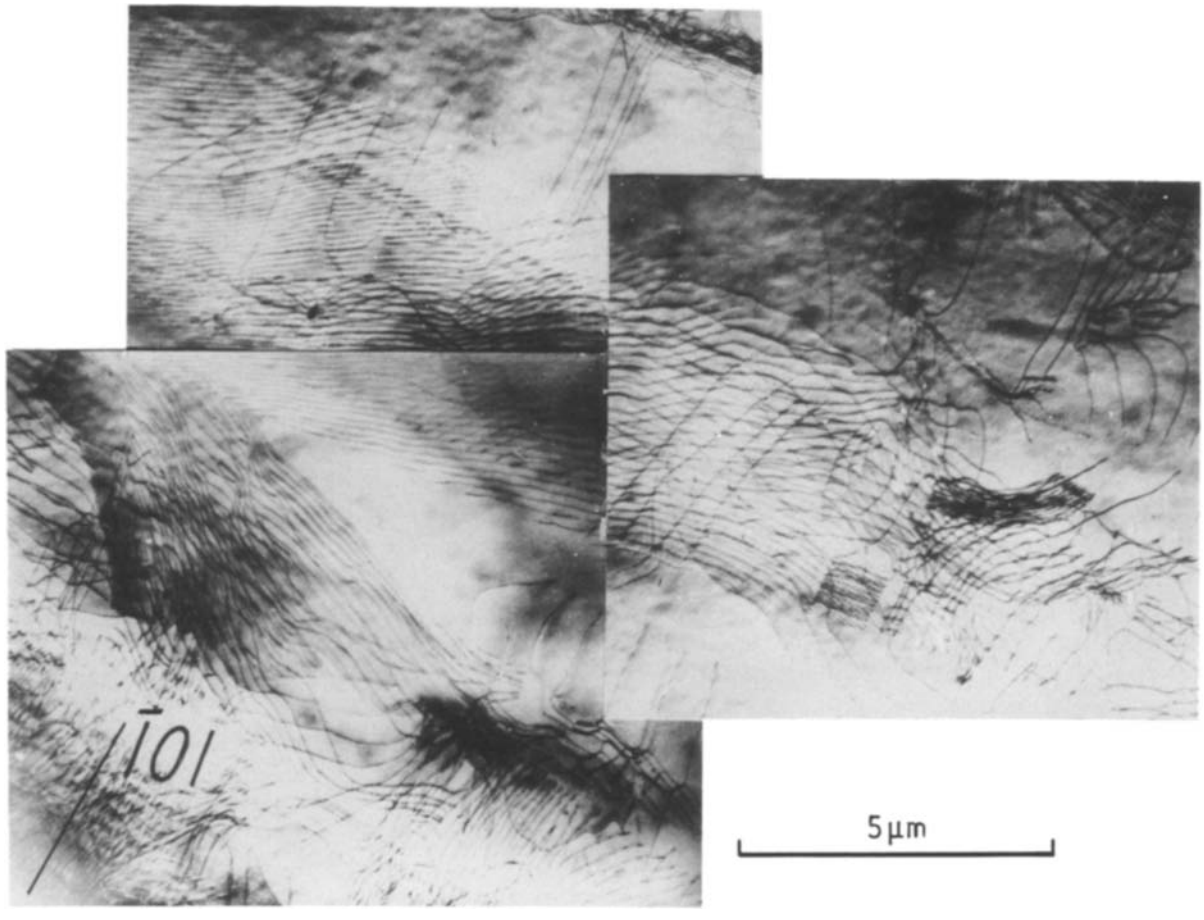

Figure 5 Transmission electron micrograph for NZ-2020 quenched from 1073 K. (1 1 1) foil.

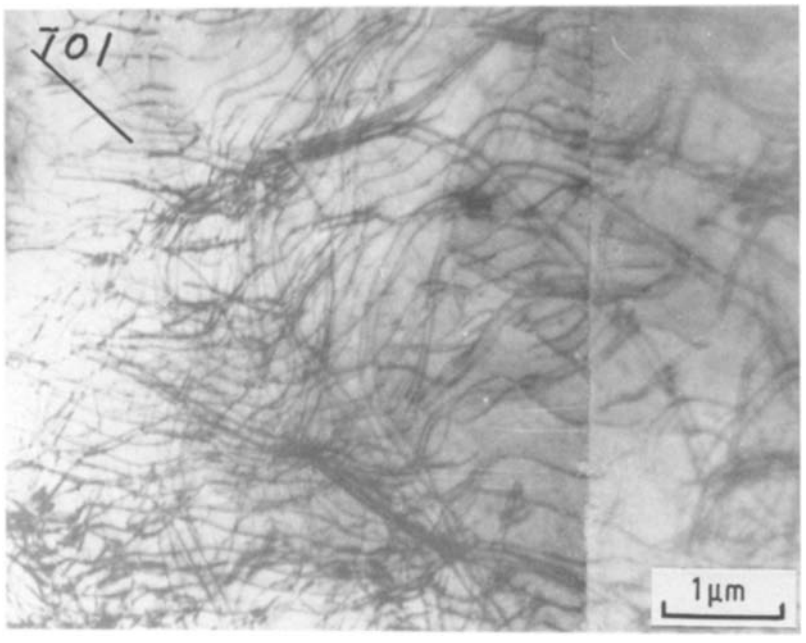

Figure 6 Transmission electron micrograph for NZ-2020 annealed at 573 K for 3.6 ksec. (1 1 1) foil.

systems is very small, and at least one order lower than that of the primary ones.

4. Discussion

The relation between the dislocation structure and the flow stress is very interesting. Fig. 10 shows the separation of edge-type superlattice dislocations forming pairs, as a function of the annealing period at 573 K. The transition from paired to unit dislocations occurs at separation ~ 150 nm. At shorter annealing periods, dislocations cannot maintain pairs and move as units. In accordance with theory, the separation for screw dislocations is about 2/3 of the measured value for the edge type [13]. The separation of a superlattice dislocation tends to decrease with the annealing period, and at the longest annealing period, ~ 35 nm for NZ-2020 and ~ 20 nm for NZ-2525 are obtained. Referring to the observations of dislocation structure, the relation between CRSS and annealing period can be explained phenomenologically according to the theory of Stoloff and Davies [14]. The abrupt increase in CRSS observed in the early part of the annealing period will correspond to the region where the dislocation movement changes from that of unit dislocations to that of pairs, corresponding to the development of a degree of order. The slow increase in the flow stress that follows will be the region where superlattice dislocations move predominantly, though still the degree of order is intermediate. The separation of dislocations forming a pair continues to decrease.

The phenomenon that the flow stress has a maximum at an intermediate degree of order has been found in FeCo–2V, Fe_3Al and Ni_3Mn [14, 15]. In Cu_2NiZn, neutron diffraction shows that the ordering reaction is very slow and it is hard to get perfect order by annealing at 573 K [1–3]. The fact that the composition of NZ-2525 deviates from that of stoichiometric Cu_2NiZn will retard the attainment of a higher

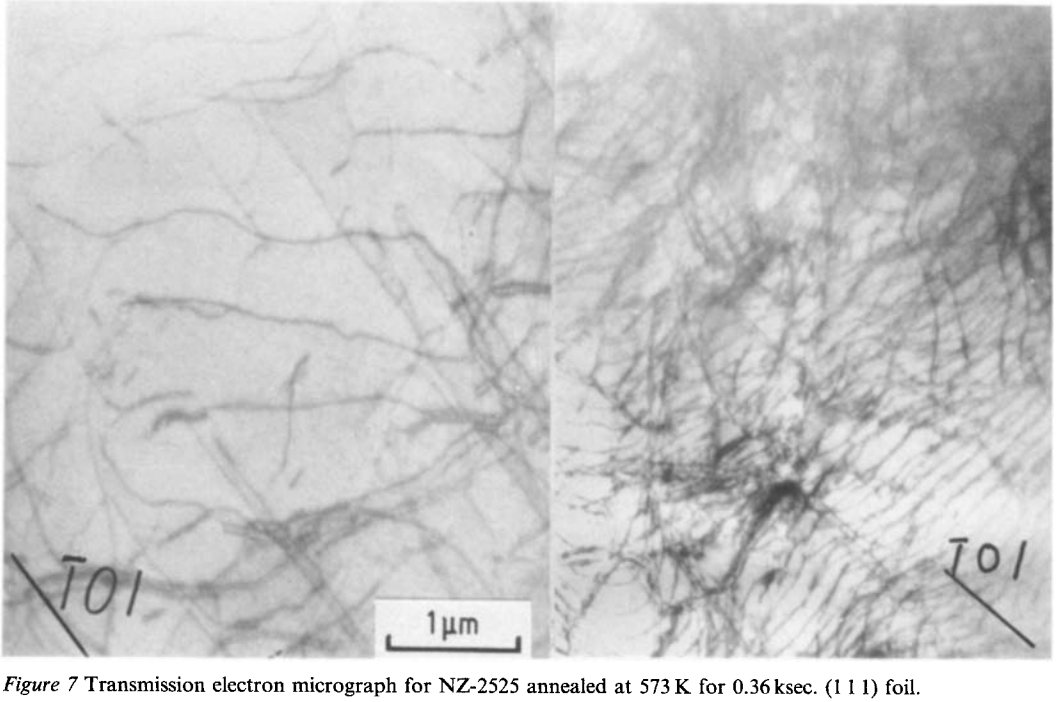

Figure 7 Transmission electron micrograph for NZ-2525 annealed at 573 K for 0.36 ksec. (1 1 1) foil.

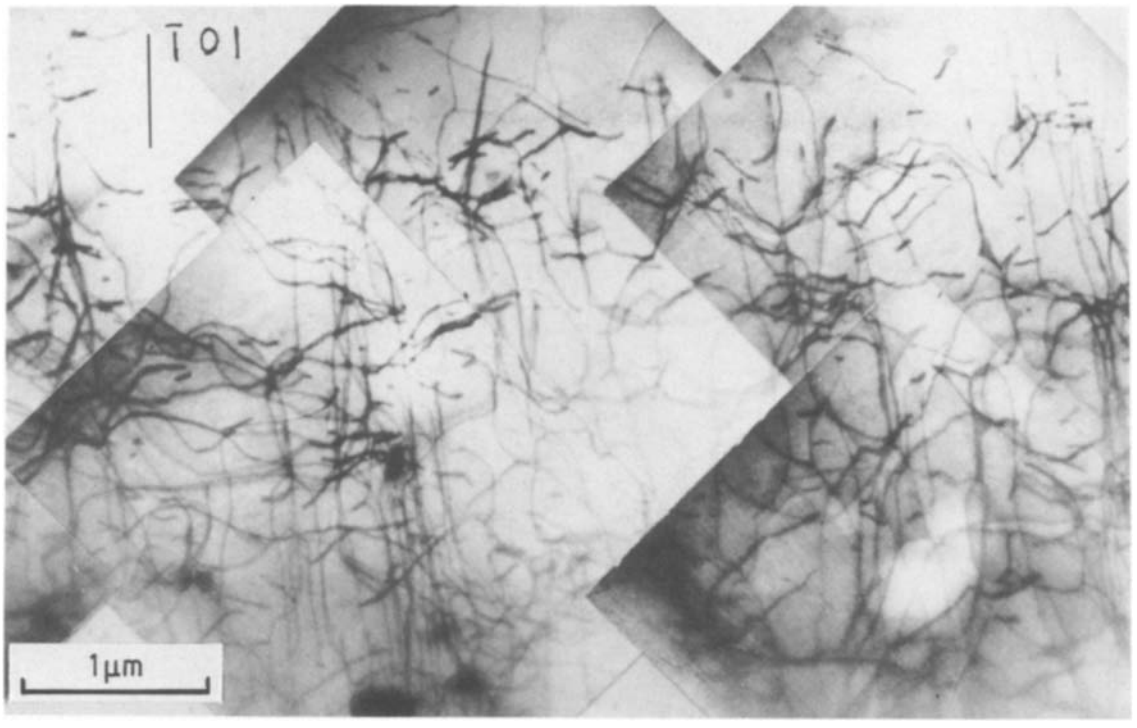

Figure 8 Transmission electron micrograph for NZ-2525 annealed at 573 K for 360 ksec. (1 1 1) foil.

degree of order. It has been reported [8] for polycrystalline Cu_2NiZn with a composition close to stoichiometry that by annealing at 623 K the flow stress had a maximum at 36 ksec and is decreased by annealing for 3600 ksec. Therefore, if a sufficient degree of order is attained the flow stress may decrease on longer annealing.

There are several mechanisms to explain the work-hardening of ordered alloys. The elastic interaction of superlattice dislocations on nearby slip planes [8], the formation of sessile antiphase domain tubes due to interaction with secondary dislocations [16], and the cross-slip of superlattice dislocations to the {1 0 0} plane [17], will be possible work-hardening mechanisms in Ll_2 type superlattices.

In the ordered NZ-2020 and NZ-2525, debris and cusps observed parallel to edge dislocation dipoles will be formed by the interaction of dislocations and will act as a barrier to moving dislocations. Therefore, their origin will give us information on the mechanism of work-hardening. Debris and cusps have been observed in β-CuZn single crystals [18] and their origin was explained by the climb of superlattice dislocation dipoles on nearby slip planes. As observed in Fig. 9, strong interactions between primary edge dislocations on nearby slip planes are observed. In contrast, the secondary dislocation density is very small, and almost all the dislocations are primary ones. Superlattice dislocation dipoles with a small distance probably change to debris and cusps, aided by climb. The authors do not have quantitative information on the stress necessary to pass over two superlattice dislocations

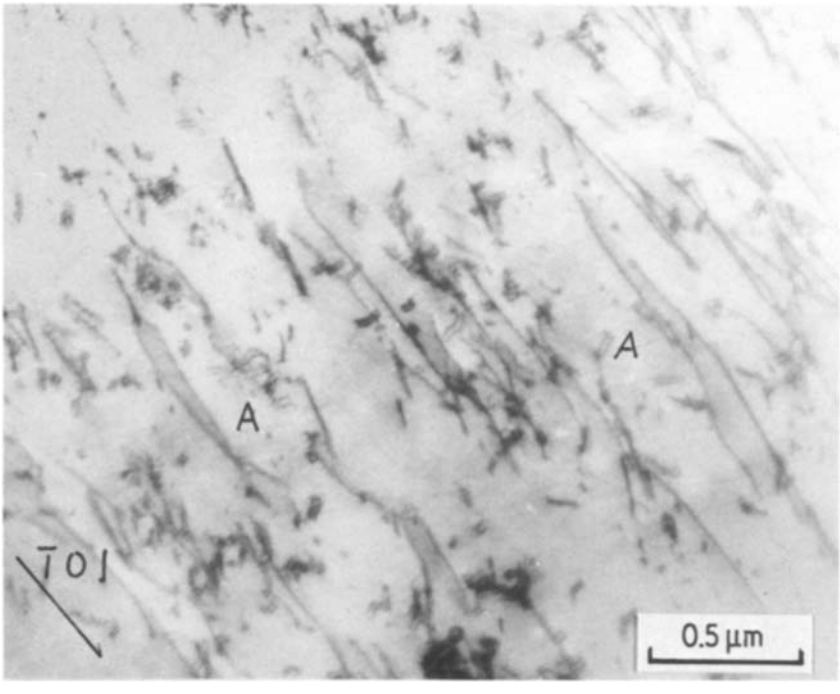

Figure 9 Transmission electron micrograph for NZ-2525 annealed at 573 K for 360 ksec. (1 $\bar{1}$ 1) foil.

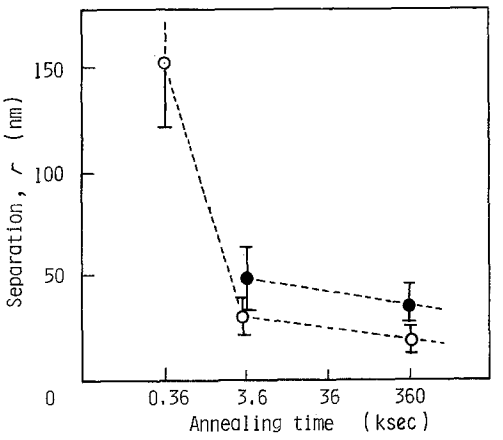

Figure 10 The relation between separation of superlattice dislocations and annealing period at 573 K for (●) NZ-2020 and (○) NZ-2525.

with different signs on parallel slip planes. To explain the work-hardening in Cu_2NiZn polycrystals, the elastic interaction between two dislocations on parallel slip planes has already been calculated [8]. Therefore, it is considered that the prominent mechanism controlling the work-hardening of ordered Cu_2NiZn single crystals is the elastic interaction of primary dislocations on parallel slip planes.

In superlattices with a high antiphase boundary energy such as Ni_3Al, the separation of dislocations forming a pair is small and screw segments of superpartials can cross-slip to the {1 0 0} plane, leaving sessile points there where debris can be formed [19, 20]. In the present alloys the separation of superpartials is rather large, ~20 nm, and each partial extends because of low stacking-fault energy. Therefore, cross-slip of moving superpartials on to the {1 0 0} plane will not occur so frequently, whether with the identical path or a different path.

In f c c metals and alloys, the secondary dislocation density is believed to be almost the same as the primary dislocation density at the end of State 1 [21]. It was found recently, in some ordered alloys such as Fe_3Al [22], β-CuZn [18] and Ni_3Fe single crystals [23], that the secondary dislocation density is far less than the primary one. In ordered Cu_2NiZn single crystals, stress–strain curves show the work-hardening rate to be higher than that of disordered Cu_2NiZn, from the beginning of plastic deformation [4]. Nevertheless, the secondary dislocation density is at least one order smaller than the primary one. The fact that deformation proceeds uniformly will be closely related to the small density of secondary dislocations, because there will be no large stress concentrations. Therefore, the short-range interaction of the primary dislocations with the secondary ones, sessile jog formation, will not be sufficiently frequent to explain the work-hardening rate.

References

1. M. HIRABAYASHI, S. HOSHINO and K. SATO, *J. Phys. Soc. Jpn* **20** (1965) 381.
2. J. VRIJEN, P. M. BRONSVELD, G. Van Der WEGEN and S. REDELAAR, *Z. Metallkde* **67** (1976) 473.
3. G. Van Der WEGEN, R. HELMHOLDT, P. BRENSVELD and J. De HOSSON, *ibid.* **74** (1983) 592.
4. S. YOSHIOKA, Y. NAKAYAMA and T. ITO, *J. Jpn Inst. Metals* **33** (1969) 557.
5. S. YOSHIOKA, Y. NAKAYAMA, T. ITO and K. FUKUNAGA, *ibid.* **37** (1973) 1243.
6. T. ITO and Y. NAKAYAMA, *Trans. Jpn Inst. Metals* **21** (1980) 745.
7. G. Van Der WEGEN, P. M. BRONSVELD and J. De HOSSON, *Met. Trans.* **12A** (1981) 2125.
8. P. M. BRONSVELD, B. RAMASWAMI, G. Van Der WEGEN and J. De HOSSON, *Acta Metall.* **30** (1982) 581.
9. G. Van Der WEGEN, P. M. BRONSVELD and J. De HOSSON, *ibid.* **30** (1982) 1537.
10. T. TAOKA and S. SAKATA, *ibid.* **5** (1957) 61.
11. T. TAOKA and R. HONDA, *J. Electron Microsc.* **5** (1957) 19.
12. R. W. K. HONEYCOMBE, "The Plastic Deformation of Metals", (Arnold, London, 1968) p. 33.
13. M. J. MARCHINCOWSKI, N. BROWN and R. M. FISHER, *Acta Metall.* **9** (1961) 129.
14. N. S. STOLOFF and R. G. DAVIES, *ibid.* **12** (1964) 473.
15. M. J. MARCHINKOWSKI and D. S. MILLER, *Phil. Mag.* **6** (1961) 811.
16. A. E. VIDOZ and L. M. BROWN, *ibid.* **7** (1962) 1167.
17. B. H. KEAR and H. G. F. WILSDORF, *Trans. AIME* **224** (1962) 382.
18. T. ITO and Y. NAKAYAMA, *Trans. Jpn Inst. Metals* **21** (1980) 683.
19. S. TAKEUCHI and E. KURAMOTO, *Acta Metall.* **21** (1973) 415.
20. *Idem, ibid.* **21** (1973) 683.
21. Z. S. BASINSKI and S. J. BASINSKI, *Phil. Mag.* **9** (1964) 51.
22. R. C. CRAWFORD, *ibid.* **33** (1976) 529.
23. A. KORNER, *Acta Metall.* **33** (1985) 1399.

Received 23 June
and accepted 22 September 1987